

Polarization swings in blazars

Maxim Lyutikov¹^{*} and Evgeniya V. Kravchenko²

¹*Department of Physics, Purdue University, 525 Northwestern Avenue, West Lafayette, IN 47907-2036, USA*

²*Lebedev Physical Institute, Astro Space Center, Profsoyuznaya 84/32, Moscow 117997, Russia*

Accepted ... Received ...; in original form ...

ABSTRACT

We present a model of blazar variability that can both reproduce smooth large polarization angle swings, and at the same time allow for the seemingly random behavior of synchrotron fluxes, polarization fraction and, occasionally, $\pi/2$ polarization jumps. We associate blazar flaring activity with a jet carrying helical magnetic fields and propagating along a variable direction (and possibly with a changing bulk Lorentz factor). The model predicts that for various jet trajectories (i) EVPA can experience large smooth temporal variations while at the same time polarization fraction (Π) can be highly variable; (ii) $\Pi \sim 0$ near sudden EVPA jumps of 90° , but can also remain constant for large, smoother EVPA swings; (iii) the total angle of EVPA rotation can be arbitrary large; (iv) intensity I is usually maximal at points of fastest EVPA changes, but can have a minimum. Thus, even for a regular, deterministic motion of a steadily emitting jet the observed properties can vary in a non-monotonic and/or seemingly stochastic way. Intrinsic fluctuations of the emissivity will further complicate the intensity profiles, but are expected to preserve the polarization structure.

Key words: polarization — galaxies: active — galaxies: magnetic fields — galaxies: jets

1 CORRELATED FLUX AND POLARIZATION VARIATIONS – OBSERVATIONAL OVERVIEW AND THEORETICAL MODELS

Blazars – a sub-class of active galactic nuclei (AGN) – have the orientation of their jets close to the line of sight (LoS). This makes their non-thermal radiation to be highly relativistically beamed. Their linear fractional polarization reaches values up to 50 per cent (e.g. [Lister & Homan 2005](#)) suggesting the presence of highly ordered magnetic fields in their compact regions ([Lyutikov et al. 2005](#)). Furthermore, observed behavior of polarization degree and angle suggest helical shape of these magnetic fields (e.g. [Gabuzda 1999](#); [Pushkarev et al. 2005](#); [Lyutikov et al. 2005](#)).

Blazars are observed to show high variability across the electromagnetic spectrum (e.g. [Quirrenbach et al. 1989](#); [Ulrich et al. 1997](#)). The evolution of the γ -ray, optical, radio and polarized fluxes often exhibit seemingly random behavior (e.g. [Larionov et al. 2013](#), and references therein) and in some cases might be represented by a number of isolated, individual events superimposed on a steady processes (e.g. [Marscher et al. 2008](#); [Kiehlmann et al. 2016](#)). In contrast, the optical electric vector position angle (EVPA) variations often show smooth swings of the linearly polarized radiation, with total rotations up to few radians (see Section 3 for corresponding examples). The noticeable nature of such events attracted special interest, giving birth to a large polarimetric programs, like

RoboPol ([King et al. 2014](#); [Pavlidou et al. 2014](#)), MAPCAT¹, monitoring at Steward observatory ([Smith 2016](#)), with Kanata optical telescope ([Ikejiri et al. 2011](#)), and others.

Apparent similarities of optical flux, degree of polarization and EVPA during these events, detected in different sources and their different flaring states, suggests a common mechanism being responsible for such a behavior. The general pattern includes high variability of polarization Π , which can be both higher and lower during the middle of EVPA swing, but then recovers back to the initial value, smooth and continuous change of polarization angle and peaked behavior of optical flux density. Figure 1 presents sample of such behavior. All EVPA rotation events (hereafter we refer to optical EVPA) have been detected to date only in the γ -ray loud objects, suggesting physical relation of optical and γ -ray emission sites. [Blinov et al. \(2015\)](#) note that these EVPA rotations may be produced via both random walk processes (e.g. [Marscher 2014](#)) and deterministic processes, while the latter can be connected with the strongest γ -ray flares (e.g. [Abdo et al. 2010](#); [Morozova et al. 2014](#); [Blinov et al. 2015](#); [Kiehlmann et al. 2016](#)).

A number of models attempt to explain the polarization behavior (e.g. [Bjornsson 1982](#); [Konigl & Choudhuri 1985](#); [Marscher 2014](#); [Laing & Bridle 2014](#); [Zhang et al. 2014](#)). The key approaches include many-zone emission models (in an attempt to explain nearly random behavior of some jet properties) and models that rely on regularly evolving jet parameters (in an attempt

^{*} Contact e-mail: lyutikov@purdue.edu

¹ www.iaa.es/~iagudo/research/MAPCAT/MAPCAT.html

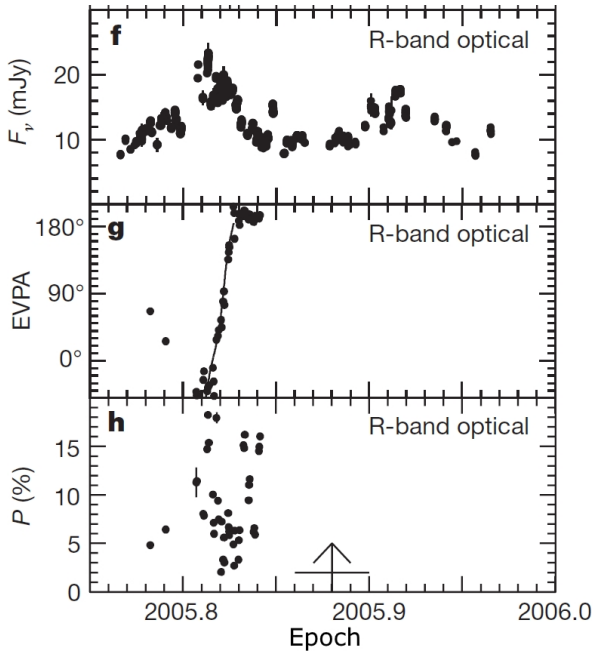


Figure 1. Optical R-band observations of BL Lac as functions of time: (f) flux density, (g) degree of polarization and (h) EVPA. Figure 2 of [Marscher et al. \(2008\)](#).

to explain smooth variations of other parameters, like the EVPA). For example, [Kiehlmann et al. \(2016\)](#) concluded that during the flare state a deterministic process governs the polarization variation, while at low-brightness state polarization is more random. The models of [Nalewajko \(2010\)](#); [Björnsson \(1982\)](#) are, perhaps, the closest to the present model.

2 THE MODEL: JET WITH HELICAL MAGNETIC FIELD PROPAGATING ALONG A VARIABLE DIRECTION

In this paper we present a model, showed in Fig. 2 - a jet propagating along a smoothly variable direction carrying helical magnetic field - which is able to reproduce large smooth variations of the EVPA, yet allow for occasional sudden jumps in EVPA. In addition - and most importantly - the intensity and polarization fraction, though produced by a highly deterministic process, show large non-monotonic variations that can be mistaken for a random process. Thus, a highly deterministic set-up of the model produces both smooth variation of EVPA and yet allows for some properties of the emission to vary in a non-monotonic way, which can be interpreted as stochastic variation.

We model the emitting element as a jet carrying helical magnetic field with internal pitch angle ψ , propagating with Lorentz factor γ_j . The jet produces polarized synchrotron emission. We concentrate on the optically thin region, sufficiently far downstream of the place, where jet originates. In terms of physical location the model is applicable to on sub-parsec to parsec scale regions of the jet. In the present paper we do not make a separation between the different parts of the spectrum, e.g. optical and radio, but outline the general properties of polarized synchrotron emission expected from a jet with variable direction.

Calculations of polarization produced by relativistically moving sources is somewhat complex ([Blandford & Königl 1979](#); [Lyutikov et al. 2003, 2005](#)).

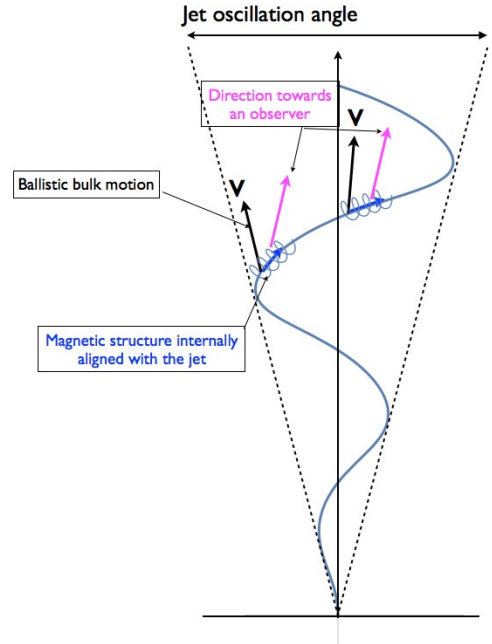


Figure 2. Schematic representation of the model. The jet is emitted along a variable direction (defined, e.g. by the opening angle of the planar motion, jets' oscillation angle). The internal helical structure of the magnetic field within the jet is aligned with the local jet direction and changes with time.

[Lyutikov et al. 2003, 2005](#)). Conventionally (and erroneously for a relativistically moving plasma!), the direction of the observed polarization for optically thin regions and the associated magnetic fields are assumed to be in one-to-one correspondence, being orthogonal to each other, so that some observers choose to plot the direction of the electric vector of the wave, while others plot vectors orthogonal to the electric vectors and call them the direction of the magnetic field. *This is correct only for non-relativistically moving optically-thin sources, and thus cannot be applied to AGN jets.* Since the emission is boosted by the relativistic motion of the jet material, *the EVPA rotates parallel to the plane containing the line of sight and the plasma velocity vector*, so that *the observed electric field of the wave is not, in general, orthogonal to the observed magnetic field*, ([Lyutikov et al. 2003, 2005](#)).

We consider the synchrotron emission of an unresolved, thin, circular cylindrical shell populated by relativistic electrons with a power law distribution and moving uniformly in the axial direction with constant velocity. The properties of the synchrotron emission are then determined by *three parameters*: the internal pitch angle of the magnetic field ψ' , Lorentz factor of the shell in the laboratory frame γ_j and the viewing angle, θ , which the line of sight to the observer makes with the jet axis in the observer reference frame. Thus, even for fixed internal parameters of the jet, the resulting polarization signature strongly depends both on the viewing angle and the jet Lorentz factor ([Lyutikov et al. 2005](#)), Fig. 3.

As a novel feature, we allow parameters of the model (the viewing angle and the Lorentz factor) to vary smoothly with time and we analyze the resulting correlations. As a result of relativistic boosting, at different moments in time the jet is seen from highly variable directions in the jet's frame. The observed intensity, polarization and EVPA then experience large variations. Even though these variations are highly correlated, the observed properties show

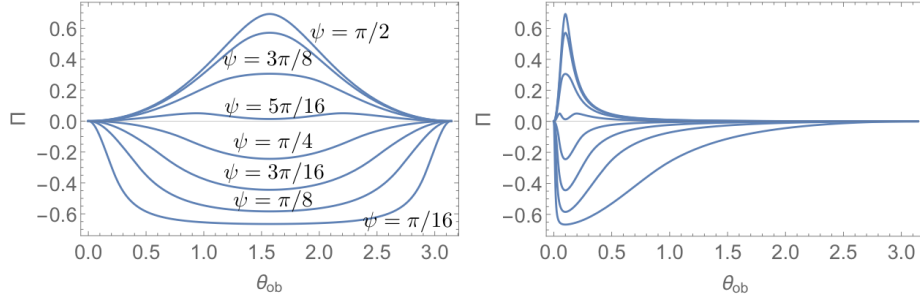


Figure 3. Polarization fraction Π for a jet carrying helical magnetic field as function of viewing angle in comoving (left panel) and observer frames (right panel, $\gamma = 10$) for different pitch angles (Lyutikov et al. 2005). Positive values correspond to average polarization along the jet, while negative correspond to polarization perpendicular to the jet. Pitch angles are $0, \pi/16/\pi/8 \dots \pi/2$. These values of the pitch angles are used in all the plots below.

large, seemingly random changes. We consider several types of jet variations: planar oscillating motion, circular motion, jet acceleration and combinations thereof.

The polarization direction from an unresolved jet can be either along the projection of the jet onto the plane of the sky, or perpendicular to it. Thus, as a jet's direction changes with time, the direction of polarization will also change. Most of the time, the EVPA will either be always along or across the jet. In addition, for a fairly narrow range of internal pitch angles and lines of sight a given jet can show 90° EVPA flips.

Importantly, in this paper we do not address the physical origin of the emission features. Qualitatively, we image that the jet motion is ballistic, but along time-dependent trajectories/velocities, determined by the changing condition at the location of the jet acceleration, like jet from a firehose. Emission is then produced by a feature moving along the jet. These emission features, propagating along changing direction, then can be modeled as a jet with variable direction.

2.1 Planar motion of the jet direction

Let us consider how apparent brightness, polarization fraction and EVPA change with time if the jet's direction executes a regular motion. First, consider planar motion of a jet, so that a jet oscillates with amplitude $\phi_{j,max} = \pm\pi/2$ making the minimum angle with the LoS $\theta_{ob,0}$, Fig. 4.

The angle θ_{ob} between the LoS and the jet direction is $\cos \theta_{ob} = \cos \theta_{ob,0} \cos \phi_j$. The angle between a fixed direction and the projection of the jet on the plane of the sky is

$$\sin \phi_{PA} = \frac{\sin \phi_j}{\sqrt{1 - \cos^2 \theta_{ob,0} \cos^2 \phi_j}} \quad (1)$$

(the EVPA can be different from (1) by $\pi/2$). The rate of change of ϕ_{PA} is:

$$\dot{\phi}_{PA} = \frac{\sin(\theta_{ob,0})}{1 - \cos^2(\phi_j) \cos^2(\theta_{ob,0})} \dot{\phi}_j \quad (2)$$

Thus, the fastest rate of EVPA swing occurs at $\phi_j = 0$. (This reasoning *excludes* possible fast $\pi/2$ polarization jumps associated with transitions through $\Pi = 0$, see below.) Also, the rate of EVPA swing (2) is expressed in terms of the coordinate time (and the coordinate rate $\dot{\phi}_j$). In terms of the observer time these rates will be modified by the time-of-travel effects. In the present paper we concentrate on the overall properties of intensity and polarization and

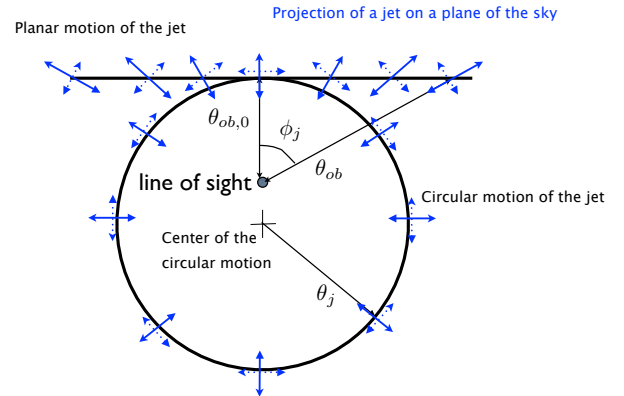


Figure 4. Geometry of the model in the plane of the sky. Direction of the jet changes with time executing planar or circular motion. Solid blue arrows represent the projection of the jet on the plane of the sky. At each point EVPA is either along or perpendicular (dotted arrows) to the projection of a jet on the plane of the sky. Fastest rate of EVPA change occurs near the closest approach between the line of sight and the jet direction. Depending on the parameters EVPA can flip by 90° . During such flips polarization will pass through zero.

neglect these effects. They will be addressed in a forthcoming paper.

In Figs. 5-6-7, we plot the polarization signatures assuming that the motion of the jet is symmetric with respect to the line of sight and that oscillations occur between angles $-\pi/2 < \phi_j < \pi/2$. We note, for $\Pi > 0$ the polarization is along the jet, while the polarization is orthogonal to the jet for $\Pi < 0$. In Fig. 8 we plot the observed intensity as a function of the oscillation angle and as a function of the EVPA of polarization.

There are two types of fast EVPA variation: (i) when the jet passes close to the line of sight, EVPA experiences fast smooth variations that can approach π radians; (ii) occasionally EVPA experiences sudden jumps by $\pi/2$ radians (Fig. 9). During such jumps the polarization fraction passes through zero.

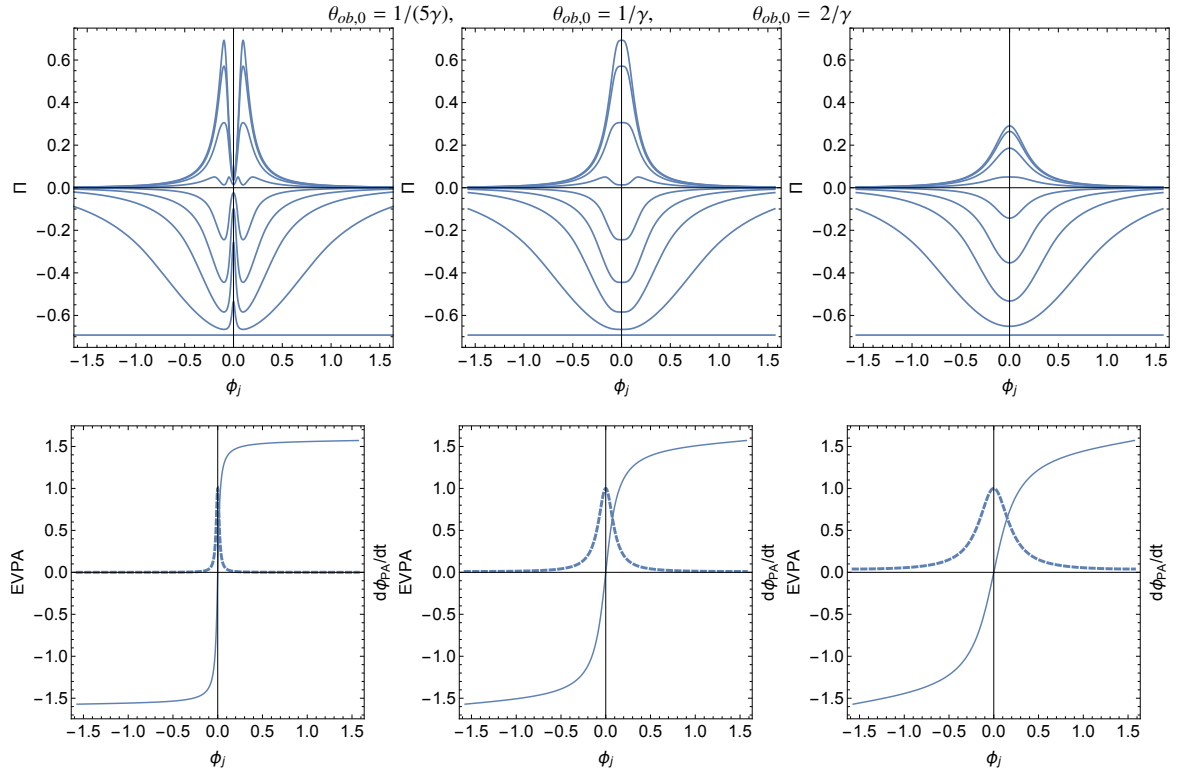


Figure 5. Polarization Π and EVPA for a jet executing planar motion. The jet is moving with bulk Lorentz factor $\gamma = 10$ and is viewed at the minimal viewing angles of $\theta_{ob,0} = 1/(5\gamma)$, $1/\gamma$, $2/\gamma$ (left to right columns). *Top row*: Π as function of the oscillation angle for different intrinsic pitch angles. *Bottom row*: EVPA as function of the oscillation angle (solid line). (Here a larger range of angles ϕ_j is plotted to show the full periodic behavior of EVPA). Dashed line: the rate of change of EVPA, ϕ_{PA} (defined here as the projection of the jet on the plane of the sky - EVPA may differ by 90°), normalized to the maximal value.

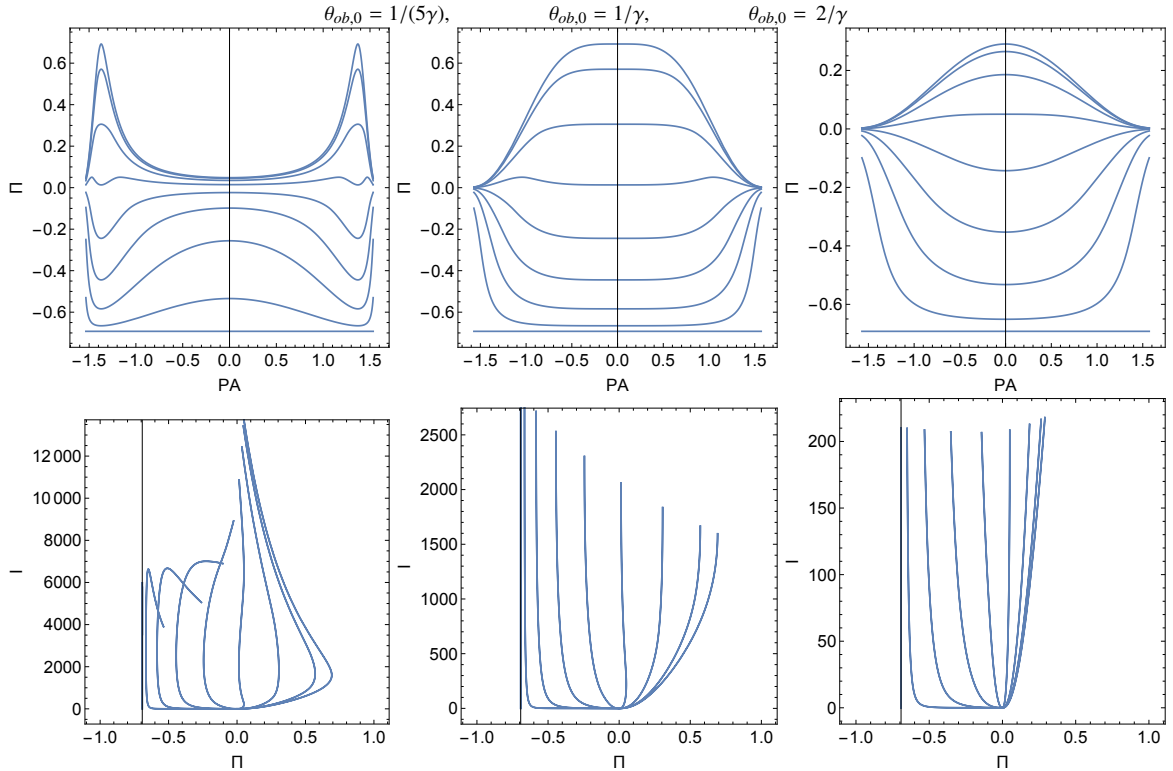


Figure 6. Same set-up as Fig. 5. *Top row*: polarization Π as function of PA. *Bottom Row*: Intensity as function of polarization degree Π .

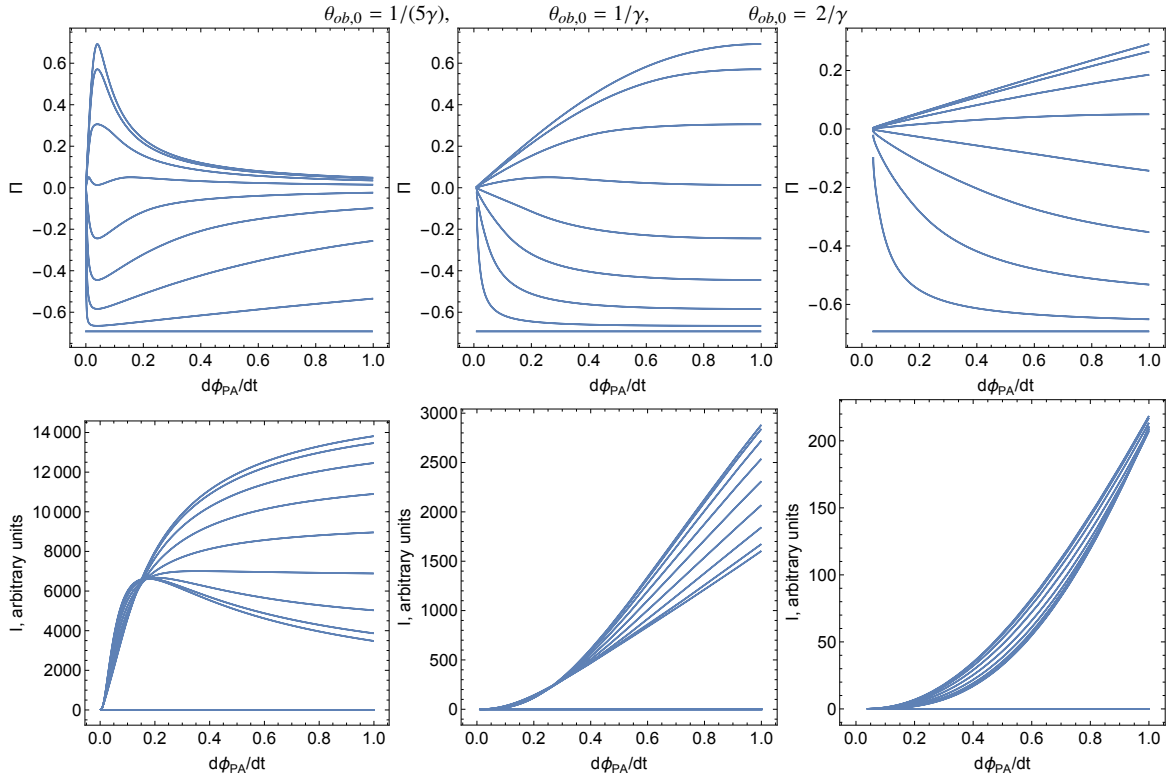


Figure 7. Same as 5. *Top row:* Polarization Π as function of $\dot{\phi}_{PA}$. Polarization can be both minimal at fastest EVPA swings (left panel) or maximal (center and right panels). For some values of the pitch angle the polarization fraction is a non-monotonic function of $\dot{\phi}_{PA}$. *Bottom row:* Intensity as function of $\dot{\phi}_{PA}$. Intensity generally increases with $\dot{\phi}_{PA}$, but can be non-monotonic (left panel). (The rate $\dot{\phi}_{PA}$ is normalized to a maximal value).

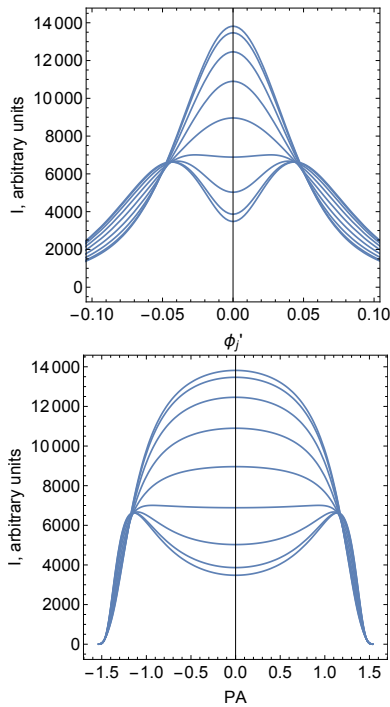


Figure 8. *Top panel:* Intensity as function of the oscillation angle (only limited range in ϕ_j is shown). For small pitch angles, and small $\theta_{ob,0}$ intensity in the middle can be low (looking almost along the magnetic field). *Bottom panel:* Intensity as function of EVPA.

2.2 Accelerating and swinging jets

Next we consider effects of jet acceleration. In Fig. 10 we plot polarization and intensity as function of the bulk Lorentz factor (left and center panels) and intensity as function of polarization fraction (right panel). Naturally, intensity is maximal when $\gamma \sim 1/\theta_{ob}$ - for smaller γ the effects of relativistic boosting are small, while for higher γ the emission is boosted away from the observer. The polarization fraction is typically smaller at lower intensities, but shows a variety of behavior.

Next we consider swinging and accelerating jets, Fig. 11. The jet executes a planar motion with amplitude $-5/\gamma_{max} < \phi < 5/\gamma_{max}$, $\gamma_{max} = 10$, while the Lorentz factor increases linearly from $\gamma = 1$ at $\phi = -5/\gamma_{max}$ to $\gamma = \gamma_{max}$ at $\phi = 5/\gamma_{max}$. The minimal viewing angle is $\theta_{ob,min} = 1/(5\gamma_{max})$. The general feature that acceleration introduces is a non-symmetric behavior of polarization with respect to the swing of EVPA.

2.3 Circular motion

Next we consider a jet executing a circular motion. Now, for a given jet Lorentz factor and minimal viewing angle $\theta_{ob,0}$ there is a parameter θ_j - the size of the circle that the jet's direction makes on the plane of the sky. Results are plotted in Fig. 12. A new feature now is that the EVPA can experience large continuous swings. The total change of EVPA is unlimited for a jet making several rotations.

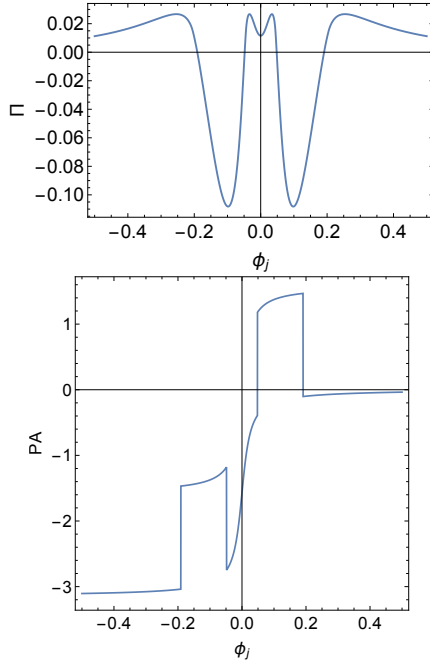


Figure 9. Polarization fraction and EVPA for $\psi = 2\pi/7$ (the direction of the jumps in EVPA are undetermined up to the factor $\pm\pi/2$); at the moment of the jump $\Pi = 0$.

2.4 Overall trends and special cases

The visual inspection of the modeling results reveals following patterns of the EVPA swings:

- Fastest swings of EVPA typically coincide with intensity and polarization extrema (maxima or minima).
- EVPA can experience fast $\pm\pi/2$ jumps near $\Pi = 0$, Fig. 9. At these points intensity can be maximal or minimal.
- Swinging jets can produce very fast EVPA swings, up to $\pm\pi$; at the maximum rate of the EVPA swings the polarization fraction minima can be maximal or minimal (first columns in Figs. 5 and 7).
- For somewhat similar intensity and polarization behaviors, the behavior of the EVPA can be high variable: smooth evolution (left panel in Fig. 12), a sudden jump (center panel in Fig. 12) or an oscillations (right panel in Fig. 12). Importantly, in most cases the fastest swing of EVPA corresponds to a minimum of polarization fraction and an extremum (maximum or minimum) in intensity. Yet, for specific case – the case of swinging jet passing along the line of sight (center column, third row, solid line in Fig. 12) – no EVPA swing is seen (corresponding to a neatly π swing in EVPA, dashed line in the same panel).
- Intensity depends on the EVPA and the polarization fraction in a complicated way; for accelerating jets such dependence is not necessarily symmetric, Fig. 11.
- Swinging jets can give EVPA rotations in opposite directions within the same source (Fig. 5, change in oscillating angle from $\pi/2$ back to $-\pi/2$).
- Circularly moving and swinging jets can produce EVPA rotations with the amplitude $\leq \pi/2$, including complex changes (e.g. Fig. 12), if a jet experience only slight changes in its direction.

We stress that these very complicated, apparently random, and yet correlated variations of intensity, polarization fraction and EVPA swings come from the assumed highly regular jet motion

Table 1. Detected to date EVPA rotations in blazars. See also Table 2.

Blazar name (B1950)	Amplitude of rotation (deg)	Reference
PKS 0420–014	–110	D’Arcangelo et al. (2007)
S5 0716+71	+180	Larionov et al. (2013)
S5 0716+71	+180	Chandra et al. (2015)
	–180	–//–
	+300	Larionov et al. (2016)
	+300	–//–
OJ 287	–180	Kikuchi et al. (1988)
S4 0954+65	+330	Morozova et al. (2014)
	–330	–//–
W Comae	+110	Benítez et al. (2013)
3C 279	~90	Abdo et al. (2010)
		Kiehlmann et al. (2016)
3C 279	–290	Larionov et al. (2008)
3C 279	–500	Kiehlmann et al. (2016)
	–100	–//–
	+350	–//–
PKS 1510–089	+720	Marscher et al. (2010)
PKS 1510–089	+400	Aleksić et al. (2014b)
PKS 1510–089	–250	Sasada et al. (2011)
	+500	–//–
BL Lac	+220	Marscher et al. (2008)
BL Lac	+210	Sillanpää et al. (1993)
CTA 102	–180	Casadio et al. (2015)
3C 454.3	+130	Sasada et al. (2010)
3C 454.3	–500	Sasada et al. (2012)
	+400	–//–

and very regular jet structure. Most importantly, we assumed *constant* jet emissivity. We expect that variations in the acceleration/emissivity properties of the jets will further complicate the observed properties. As well as more complicated trajectories of a beam can give more complicated profiles.

3 COMPARISON WITH OBSERVATIONS

The number of detected EVPA rotations to date (at least those which we known) accounts 52 in 20 blazars (see Table 1 and Table 2) and are observed to occur on dramatically different time scales – from days to months. The amplitude of a majority of these rotations lies in range from 70° to 360° , while larger rotations have also been observed.

The bulk of these rotations possesses the same properties (though more complex behavior is observed):

- degree of polarization is highly variable (e.g. Sasada et al. 2012), while during the EVPA swing Π is lower than during the intervals with no rotations (e.g. Blinov et al. 2016);
- EVPA changes smoothly and exhibits small variations around some mean value during the quiescent state of the source (e.g. Abdo et al. 2010);
- the fast changes in EVPA seem to occur when polarization fraction passes through minimum (e.g. Blinov et al. 2016);
- total optical flux experiences flares or doesn’t change at all.

3.1 Fast $\pm 180^\circ$ rotations

Nearly sixty per cents of observed rotational events have maximum amplitude of EVPA change $\leq 180^\circ$. Since our model explains

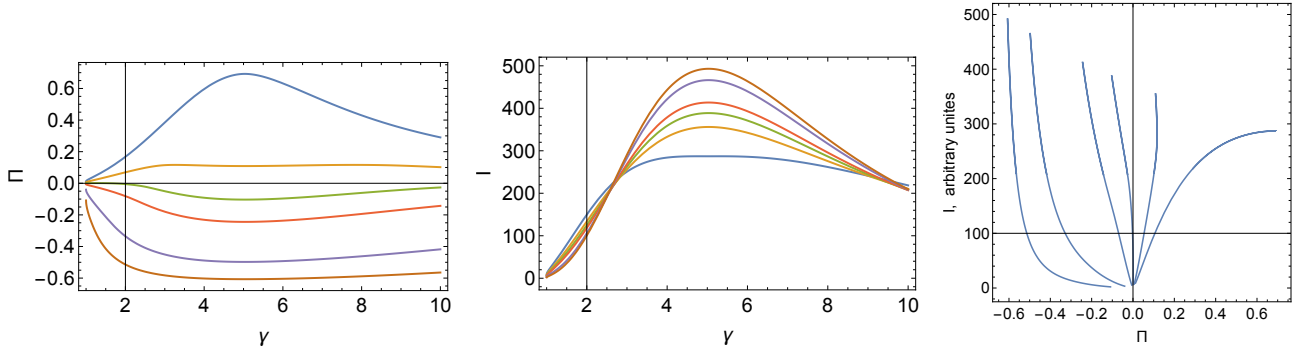


Figure 10. Polarization Π (left panel) and intensity I (center panel) as function of bulk Lorentz factor γ for accelerating jet. Intensity as function of polarization (right panel). Viewing angle $\theta_{ob} = 0.2$. Different curves correspond to different intrinsic pitch angles.

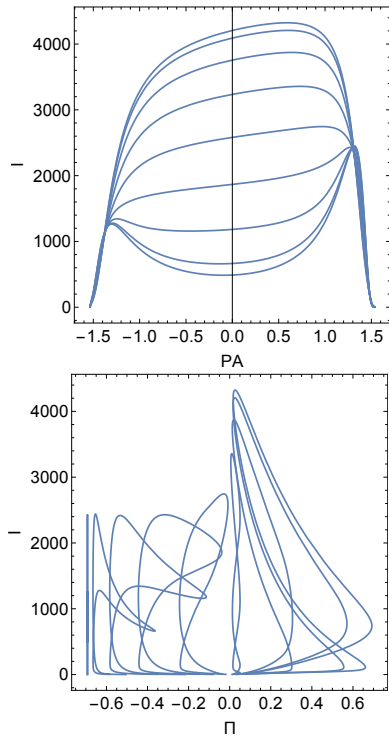


Figure 11. Swinging and accelerating jets. Shown are intensity as function of the EVPA (top panel) and polarization fraction (bottom panel). Though in most cases peak intensity coincides with minimal Π , there are clear exceptions, when polarization can be maximal at the peak of intensity, or be flat.

Table 2. Detected EVPA rotations in blazars within RoboPol monitoring program.

Blazar name (B1950)	Amplitude of rotation (deg)	Reference
OC 457	−225	Blinov et al. (2015)
	−92	Blinov et al. (2016)
PKS 0256+71	−180	Blinov et al. (2015)
S5 0716+71	−208	—
OJ 287	−154	—
GB6 J1037+5711	−165	Blinov et al. (2016)
S4 1044+71	−188	Blinov et al. (2015)
PKS 1510−089	+243	Blinov et al. (2016)
	−200	—
PG 1553+113	+128	Blinov et al. (2015)
	+145	Blinov et al. (2016)
TXS1557+565	+222	Blinov et al. (2015)
S4 1749+70	−126	Blinov et al. (2016)
OT 081	−335	—
S5 1803+784	−192	—
3C 371	−347	Blinov et al. (2015)
	+238	—
	−187	Blinov et al. (2016)
S4 1926+61	−105	Blinov et al. (2015)
S5 2023+760	+107	Blinov et al. (2016)
BL Lac	−253	Blinov et al. (2015)
CTA 102	−312	—
	−140	—
RGB J2243+203	−183	—
3C 454.3	−129	—
	+145	Blinov et al. (2016)
B2 2308+34	+74	Blinov et al. (2015)

complex behavior of fast $\pm 180^\circ$ rotations, we consider here only few EVPA rotational events. One particularly interesting source is S5 0716+71, in which four $\pm 180^\circ$ rotational events have been registered to date (Larionov et al. 2013; Chandra et al. 2015; Blinov et al. 2015). The complex, seemingly erratic behavior of the degree of polarization in 2015 in the source (Chandra et al. 2015), given in Fig. 13, is accompanied by smooth clockwise rotation of the optical EVPA with 180° , which then changes the direction and rotates back with the same amplitude. Such behavior, as well as EVPA swings in 2011 (Larionov et al. 2013) and 2013 (Blinov et al. 2015) may be explained by the proposed model (Fig. 5, right row), if S5 0716+71 jet experiences regular changes in its orientation. Indeed, Britzen et al. (2009), Lister et al. (2013) and Rani et al. (2014) report about S5 0716+71 parsec-scale jet variations,

showing correlation with the radio and γ -ray flaring activity Rani et al. Their analysis supports our idea about the main contribution of a variations in S5 0716+71 jet direction to the observed outburst behavior.

Other interesting source is BL Lac, which is observed to show fast EVPA swing events ($+210^\circ$, Sillanpää et al. (1993); $+220^\circ$, Marscher et al. (2008); -253° , Blinov et al. (2015)), examples of which are presented in Fig. 1. Observed behavior of these EVPA rotations is very close to the predictions of the proposed model (Fig. 5), suggesting structural changes in the jet of BL Lac. Indeed, Stirling et al. (2003) and Caproni et al. (2013) show that the BL Lac jet oscillates on the plane of the sky (see Fig. 14), which supports our assumptions.

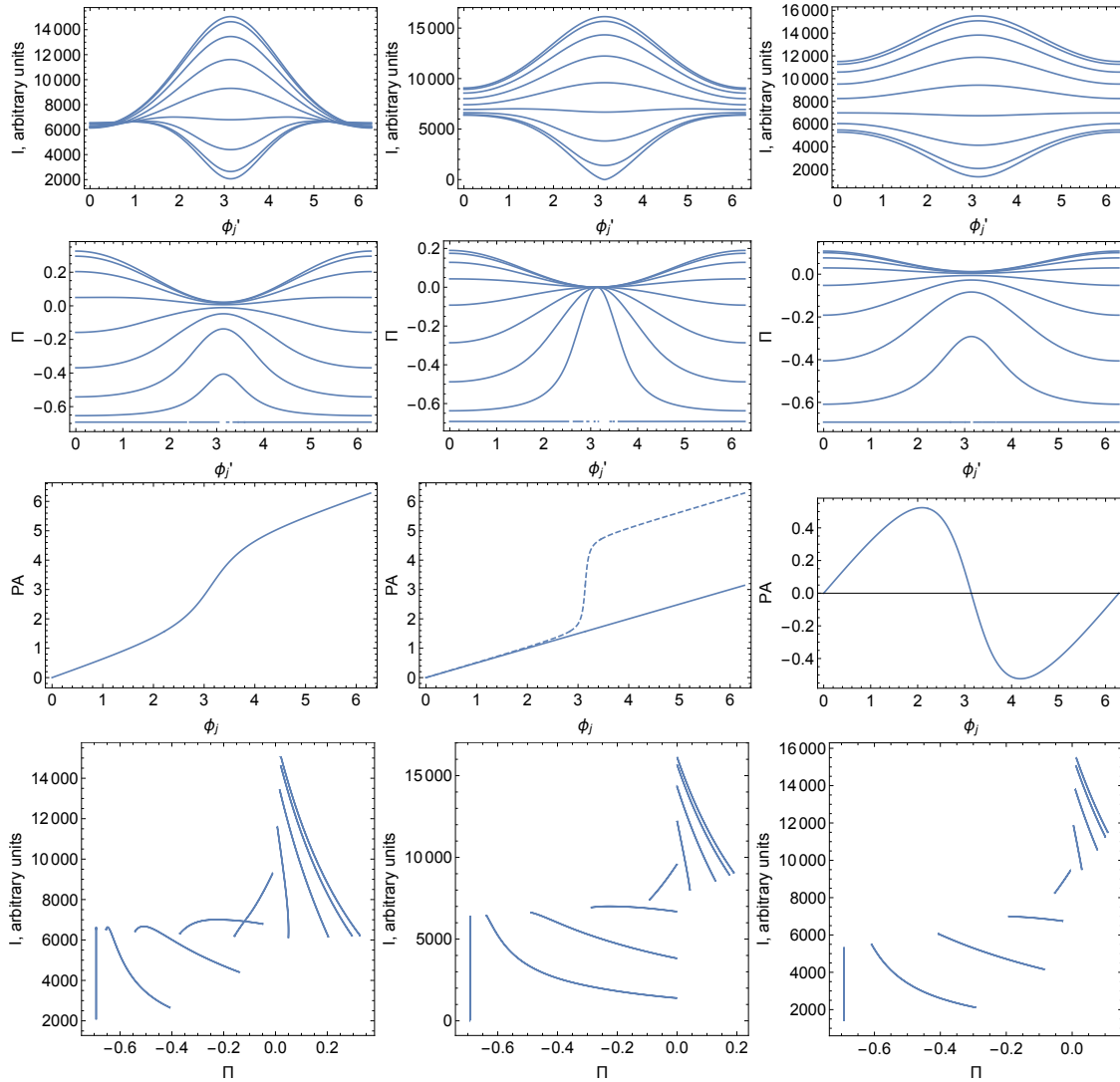


Figure 12. Intensity (first row) and polarization (second row) and EVPA (third row) as function of the jet direction for a jet executing a circular motion. Fourth row: polarization as function of intensity. Jet Lorentz factor is $\gamma = 10$, viewing angle $\theta_{ob,min} = 0.02$. The jet makes a circle with opening angle $\theta_j = 0.03$ (left column), $\theta_j = 0.02$ (center column, so that sometimes the line of sight is directed along the jet) and $\theta_j = 0.01$. The dashed line (second column, third row) indicates that when jet direction passes close to the line of sight the EVPA actually experiences $\sim \pi$ swing (it is unobservable for exact alignment). Polarization has minimum and intensity is maximal when the rate of EVPA swing is maximal.

3.2 Large EVPA rotations (jet's circular motion)

Other forty per cents of the observed rotational events have maximum amplitude of EVPA change higher than 180° , including six events with the rotation $> 360^\circ$. Deviation of the observed amplitudes of EVPA changes from 180° and 360° indicates that EVPA can make non-integer number of turns around the line of sight, accompanied by a partial or sequential Π , EVPA and I patterns, predicted by the model. Jets of, for example, CTA 102 (Blinov et al. 2015; Casadio et al. 2015), TXS 1557+565 (Blinov et al. 2015), 3C 371 (Blinov et al. 2015), 3C 279 (Kiehlmann et al. 2016) and others, might be considered to exhibit circular motion.

The largest EVPA swing to date is observed in PKS 1510–089 (Marscher et al. 2010) and amounts 720° . Assuming circular motion of the blazar jet, this overall rotation might be represented by a sequence of 180° – 360° EVPA turns. Other five detected rotational events in this blazar (Sasada et al. 2011; Aleksić et al. 2014b; Blinov et al. 2015, 2016) have amplitudes from 200° to 500° and oc-

cur in different directions (Fig. 15 shows an example of blazar activity in 2014). These continuous EVPA variations imply that the PKS 1510–089 jet executes irregular, circular motion. Different emission features, rotating in opposite directions relative to the line of sight, or close proximity of the jet viewing angle to the LoS may be responsible for the complex blazar flaring behavior in time.

Blazar 3C 454.3 also experiences large EVPA rotational events (see Table 1 and Table 2). Its jet shows complex VLBI structure (e.g. Jorstad et al. 2005) with the indication of a very small angle of jet direction to the line of sight. This may explain complex overall behavior of its properties during both active and quiescent states. Considering the 3C 454.3 jet executing a circular motion, which in a sky projection turns into planar motion in some cases, our model may explain its observed overall properties: fast EVPA swings with the amplitude less than 180° (Sasada et al. 2010; Blinov et al. 2015, 2016) as well as large and continuous EVPA rotations (-500° and $+400^\circ$, Sasada et al. 2010, 2012).

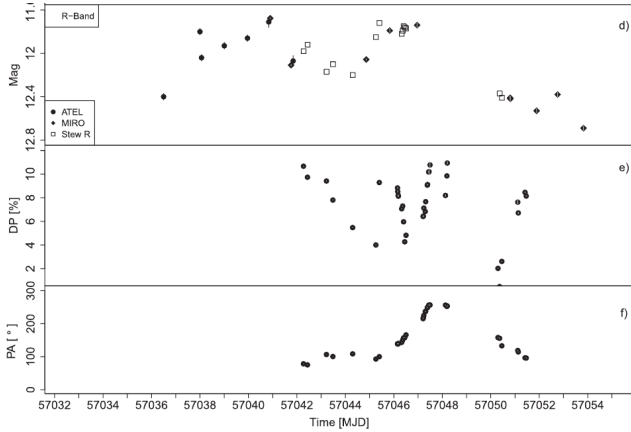


Figure 13. From top to bottom: UV/optical magnitudes, degree of polarization and EVPA of S5 0716+71 during 2015, January. Figure 1 of Chandra et al. (2015).

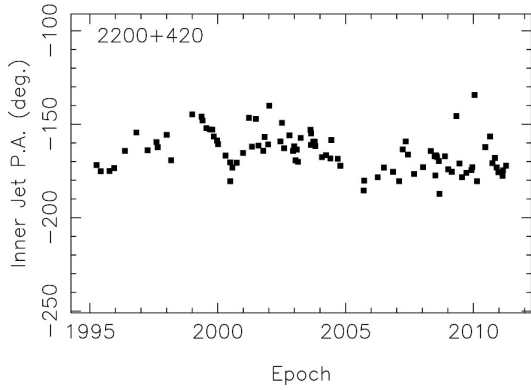


Figure 14. Innermost jet position angle vs. time, observed within VLBA MOJAVE program at 15 GHz for BL Lac. Figure 7 of Lister et al. (2013).

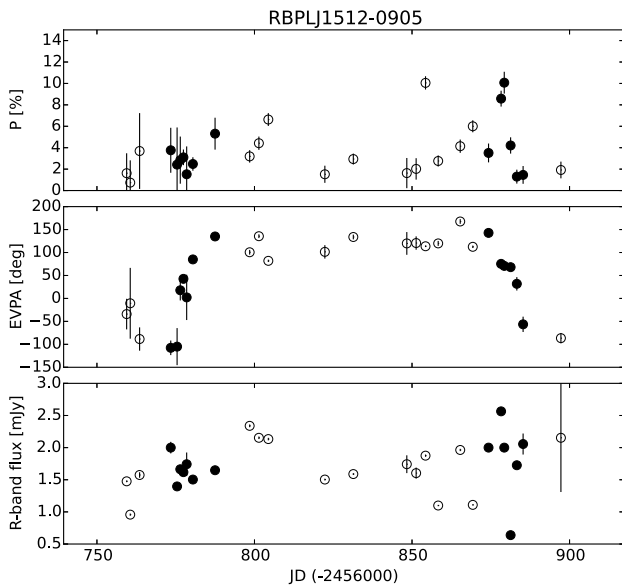


Figure 15. From top to bottom: evolution of polarization degree, EVPA and R-band magnitude for PKS 1510-089 with a detected EVPA rotation in the RoboPol monitoring program. Periods of rotations are marked by filled black points. Figure 3 of Blinov et al. (2016).

Another source exhibiting a number of different EVPA rotations, is 3C 279. The largest rotation in its jet amounts 500° (counterclockwise rotation, Kiehlmann et al. 2016) and occurs during the quiescent state of the source, shown in Fig. 16. Kiehlmann et al. (2016) conclude that the stochastic process is responsible for this rotation. We argue, that the model of a circular motion of a jet can reproduce observed properties of this EVPA rotational event (Fig. 12), resulted in relatively constant optical flux, zero degree of polarization and continuous change of EVPA. The small, short-term fluctuations overlaid on this 500° rotation may arise from the turbulent component of magnetic field, superimposed with a large scale ordered magnetic field. Or being due to small-amplitude random short-term “jitter” of the jet’s direction, superimposed on a continuous longer term evolution. Properties during the other EVPA rotations in this source (Larionov et al. 2008; Aleksić et al. 2014a; Kiehlmann et al. 2016) also can be interpreted within proposed model, including the complex $\sim 90^\circ$ rotation in 2009 (Abdo et al. 2010; Kiehlmann et al. 2016), represented in Fig. 17.

3.3 Complex EVPA rotations

In some cases the EVPA shows complex behavior, as discussed above 3C 279. The other example is the flare in S5 0954+65 in 2011 (Morozova et al. 2014), Fig. 18. EVPA steadily increases from 0° to 330° and then recovers back to 0° , accompanied by strong variations in optical flux density and fractional polarization. Morozova et al. (2014) explains such activity by a superposition of two radiative components, with only one component is responsible for EVPA rotation. Applying this explanation to the predictions of our model, one may expect, that the jet of S5 0954+65 experiences oscillating circular motion.

4 DISCUSSION

In this work we discuss a model of blazar activity - a jet carrying helical magnetic field with a regularly changing direction (and possibly changing bulk Lorentz factor) and constant emissivity. We demonstrate that this highly deterministic model can produce highly variable polarization, EVPAs, and intensity profiles. At the same time the model reproduces smoothly varying EVPA changes. Thus, though for any given configuration the intensity, polarization and the EVPA are deterministic and thus their behavior is highly correlated, the non-monotonic variations of these values as functions of the jet direction and Lorentz factor produce highly variable overall behavior. We find that for smooth variation of EVPA (i) Π can be highly variable; (ii) Π is close to zero at the moment of fastest EVPA swing; (iii) the intensity is usually maximal at points of fastest EVPA swing, but can have a minimum; (iv) for some special pitch angles there are large fluctuations of EVPA, but this always occurs at small Π .

Importantly, these features are obtained for the assumed constant intrinsic jet emissivity. Variations in the acceleration/emissivity properties of the jets, more complicated or irregular beam trajectories, as well as existence of multiple emission components within one beam will complicate observed profiles. In addition to the possible presence of a turbulent magnetic fields, these features may produce small ($< 90^\circ$), seemingly random EVPA variations (e.g. Larionov et al. 2013). Such variations are often observed during the quiescent state of the source and are not considered in this paper.

Previously, a number of models have been proposed to explain

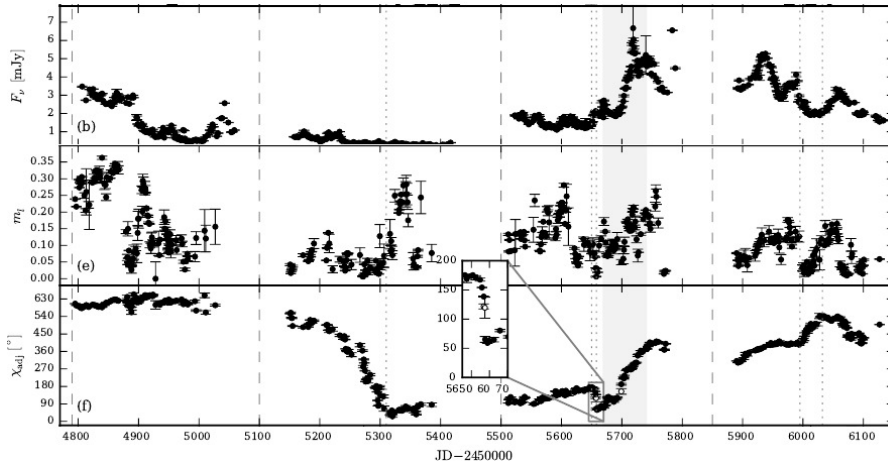


Figure 16. Optical photometry and polarimetry of 3C 279. (b) Combined R-band light curve. (e) Combined, de-biased, and averaged polarization fraction. (f) Combined, averaged, and adjusted EVPA; open symbols are added from the non-averaged EVPA curve. The grey area highlights the period of γ -ray flaring activity coinciding with a rotation of the optical polarization angle. Figure 1 of [Kiehlmann et al. \(2016\)](#).

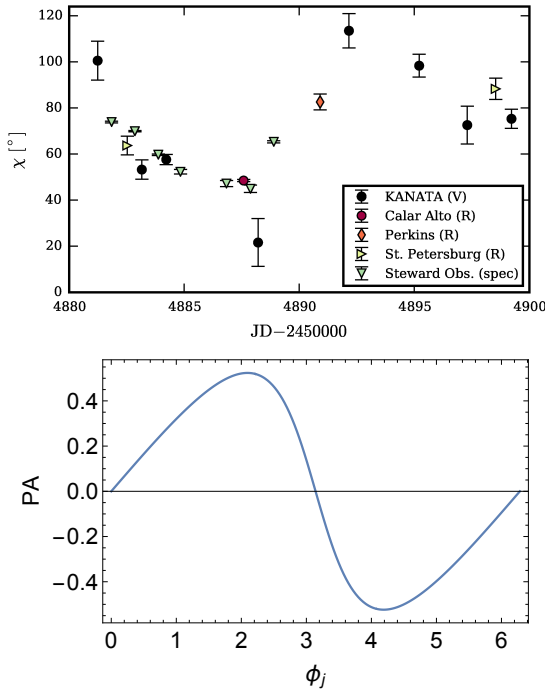


Figure 17. *Top panel:* The EVPA rotation in the jet of 3C 279 in 2009 (Fig. 3 of [Kiehlmann et al. \(2016\)](#)). *Bottom panel:* EVPA (third row right column of Fig. 12) as function of the jet direction for a jet executing a circular motion. There is apparent qualitative agreement - no fits/parameter fine tuning has been done.

blazar variability, such as propagation of the emission region along a helical ([Abdo et al. 2010](#)), spiral ([Marscher et al. 2010](#)) or bent trajectories ([Molina et al. 2014](#)), relativistic shocks propagating in a jet ([Marscher & Gear 1985](#)), interaction of the relativistically moving plasma with a standing shocks ([Marscher 2014](#)), magnetic reconnection ([Lyutikov 2003](#); [Giannios et al. 2009](#)) and passage of a disturbance through the emission region of a jet ([Zhang et al. 2014](#)). Unlike above mentioned works, the main idea of the proposed model is to interpret observed polarization and kinematic signatures of the blazar jets and not to consider physical background

of the jet emission properties and mechanisms, like particle energy distribution, acceleration and γ -ray production.

The fact that EVPA rotations have been detected only in γ -ray-loud objects suggests the better alignment of the jet-emitting regions with the line of sight during these events or large apparent speeds in these objects (e.g. [Lister et al. 2015](#)), resulting in increase of Doppler boosting factor. One may expect that within the proposed model the strongest γ -ray flares are accompanied by the fastest EVPA rotations.

We envision that changing jet direction is due to the changing launching direction, so that the motion of each element is (nearly) ballistic. The variability is then created not at the central black hole but within the flow itself. For example, we may be seeing mini-jets ([Lyutikov 2006](#); [Giannios et al. 2009](#); [Ghisellini & Tavecchio 2008](#); [Kumar & Narayan 2009](#)) that move relativistically within the overall jetted outflow. Relativistic internal sub-jets can result from reconnection occurring in highly magnetized plasma ([Lyutikov & Uzdensky 2003](#); [Hoshino & Lyubarsky 2012](#)) due to the development of current-driven instabilities (e.g. [Bromberg & Tchekhovskoy 2016](#)). The corresponding time scales in the jet frame are the dynamical (Alfvén) time of the inner part of the jet. In the observer frame the time scale will be modified by the relativistic effects, and can be considerably shorter, by a factor $1/\gamma^2$.

We would like to thank Tobias Beuchert, Sebastian Kiehlmann, Matthew Lister, Alexander Pushkarev, Hao-Cheng Zhang and the participants of the Jets2016 meeting². ML was supported by NSF grants AST-1306672 and AST-1516958.

REFERENCES

- Abdo A. A., et al., 2010, *Nature*, **463**, 919
- Aleksić J., et al., 2014a, *A&A*, **567**, A41
- Aleksić J., et al., 2014b, *A&A*, **569**, A46
- Benítez E., Sorcia M., Hiriart D., 2013, in *European Physical Journal Web of Conferences*. p. 07010, doi:10.1051/epjconf/20136107010
- Björnsson C.-I., 1982, *ApJ*, **260**, 855
- Blandford R. D., Königl A., 1979, *ApJ*, **232**, 34

² <http://jets2016.iaa.es>

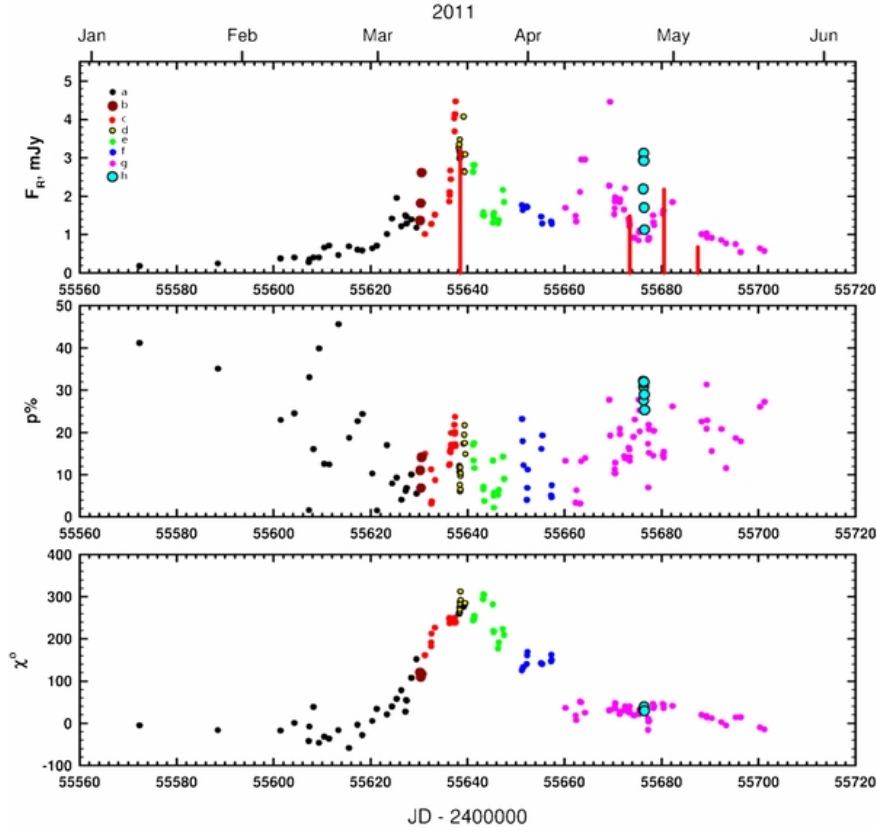


Figure 18. Optical flux density (corrected for Galactic extinction), fractional polarization, and position angle of polarization in R band vs. time in 2011 January–May in S5 0954+65, Figure 2 of [Morozova et al. \(2014\)](#).

- Blinov D., et al., 2015, *MNRAS*, **453**, 1669
 Blinov D., et al., 2016, *MNRAS*, **457**, 2252
 Britzen S., et al., 2009, *A&A*, **508**, 1205
 Bromberg O., Tchekhovskoy A., 2016, *MNRAS*, **456**, 1739
 Caproni A., Abraham Z., Monteiro H., 2013, *MNRAS*, **428**, 280
 Casadio C., et al., 2015, *ApJ*, **813**, 51
 Chandra S., Zhang H., Kushwaha P., Singh K. P., Bottcher M., Kaur N., Baliyan K. S., 2015, *ApJ*, **809**, 130
 D’Arcangelo F. D., et al., 2007, *ApJ*, **659**, L107
 Gabuzda D. C., 1999, *New Astron. Rev.*, **43**, 691
 Ghisellini G., Tavecchio F., 2008, *MNRAS*, **386**, L28
 Giannios D., Uzdensky D. A., Begelman M. C., 2009, *MNRAS*, **395**, L29
 Hoshino M., Lyubarsky Y., 2012, *Space Sci. Rev.*, **173**, 521
 Ikejiri Y., et al., 2011, *PASJ*, **63**, 639
 Jorstad S. G., et al., 2005, *AJ*, **130**, 1418
 Kiehlmann S., et al., 2016, *A&A*, **590**, A10
 Kikuchi S., Mikami Y., Inoue M., Tabara H., Kato T., 1988, *A&A*, **190**, L8
 King O. G., et al., 2014, *MNRAS*, **442**, 1706
 Konigl A., Choudhuri A. R., 1985, *ApJ*, **289**, 188
 Kumar P., Narayan R., 2009, *MNRAS*, **395**, 472
 Laing R. A., Bridle A. H., 2014, *MNRAS*, **437**, 3405
 Larionov V. M., et al., 2008, *A&A*, **492**, 389
 Larionov V. M., et al., 2013, *ApJ*, **768**, 40
 Larionov V., Jorstad S., Marscher A., Smith P., 2016, *Galaxies*, **4**, 43
 Lister M. L., Homan D. C., 2005, *AJ*, **130**, 1389
 Lister M. L., et al., 2013, *AJ*, **146**, 120
 Lister M. L., Aller M. F., Aller H. D., Hovatta T., Max-Moerbeck W., Readhead A. C. S., Richards J. L., Ros E., 2015, *ApJ*, **810**, L9
 Lyutikov M., 2003, *New Astron. Rev.*, **47**, 513
 Lyutikov M., 2006, *MNRAS*, **369**, L5
 Lyutikov M., Uzdensky D., 2003, *ApJ*, **589**, 893
 Lyutikov M., Pariev V. I., Blandford R. D., 2003, *ApJ*, **597**, 998
 Lyutikov M., Pariev V. I., Gabuzda D. C., 2005, *MNRAS*, **360**, 869
 Marscher A. P., 2014, *ApJ*, **780**, 87
 Marscher A. P., Gear W. K., 1985, *ApJ*, **298**, 114
 Marscher A. P., et al., 2008, *Nature*, **452**, 966
 Marscher A. P., et al., 2010, *ApJ*, **710**, L126
 Molina S. N., Agudo I., Gómez J. L., Krichbaum T. P., Martí-Vidal I., Roy A. L., 2014, *A&A*, **566**, A26
 Morozova D. A., et al., 2014, *AJ*, **148**, 42
 Nalewajko K., 2010, *International Journal of Modern Physics D*, **19**, 701
 Pavlidou V., et al., 2014, *MNRAS*, **442**, 1693
 Pushkarev A. B., Gabuzda D. C., Vetukhnovskaya Y. N., Yakimov V. E., 2005, *MNRAS*, **356**, 859
 Quirrenbach A., Witzel A., Krichbaum T., Hummel C. A., Alberdi A., 1989, *Nature*, **337**, 442
 Rani B., Krichbaum T. P., Marscher A. P., Jorstad S. G., Hodgson J. A., Fuhrmann L., Zensus J. A., 2014, *A&A*, **571**, L2
 Sasada M., et al., 2010, *PASJ*, **62**, 645
 Sasada M., et al., 2011, *PASJ*, **63**, 489
 Sasada M., et al., 2012, *PASJ*, **64**
 Sillanpää A., Takalo L. O., Nilsson K., Kikuchi S., 1993, *Ap&SS*, **206**, 55
 Smith P., 2016, *Galaxies*, **4**, 27
 Stirling A. M., et al., 2003, *MNRAS*, **341**, 405
 Ulrich M.-H., Maraschi L., Urry C. M., 1997, *ARA&A*, **35**, 445
 Zhang H., Chen X., Böttcher M., 2014, *ApJ*, **789**, 66

This paper has been typeset from a \LaTeX file prepared by the author.